RIGOROUS KAM RESULTS AROUND ARBITRARY PERIODIC ORBITS FOR HAMILTONIAN SYSTEMS.

TOMASZ KAPELA AND CARLES SIMÓ

Abstract. We set up a methodology for computer assisted proofs of the existence and the KAM stability of an arbitrary periodic orbit for Hamiltonian systems. We give two examples of application for systems with 2 and 3 degrees of freedom. The first example verifies the existence of tiny elliptic islands inside large chaotic domains for a quartic potential. In the 3-body problem we prove the KAM stability of the well-known figure eight orbit and two selected orbits of the so called family of rotating Eights. Some additional theoretical and numerical information is also given for the dynamics of both examples.

1. Introduction

KAM Theorem (see [14, 2, 21] and also [3]) is a fundamental result for Hamiltonian systems because it ensures the existence of a set, nowhere dense but of positive measure, of points of the phase space which behave in a regular, quasi-periodic way. The main point is that the system should be a perturbation of an integrable system and that a non-degeneracy condition, asking for the invertibility of the actions to frequencies map, has to be satisfied. The standard notation, being a Hamiltonian system given by

$$\dot{q} = H_p \qquad \dot{p} = -H_q\,, \tag{1}$$

where the Hamiltonian $H(q,p) : \Omega \to \mathbb{R}$ is a smooth function defined on an open set $\Omega \subset \mathbb{R}^{n+1} \times \mathbb{R}^{n+1}$, will be used.

If we consider the dynamics close to a fixed point the methodology is simple. Assume that the fixed point is totally elliptic or the problem can be reduced to the totally elliptic case, for instance by restricting the attention to the centre manifold. Then one can proceed to compute the normal form up to a moderate order, say to order 4 in the (q,p) variables. Assuming that no resonances occur up to this order then one can consider the normal form as the integrable Hamiltonian and the remainder as the perturbation, and it is easy to check the non-degeneracy condition. This approach has been used, e.g., in the study of the vicinity of the collinear libration points in the general planar three-body problem, restricted to the centre manifold, see [17]. A moderate number of arithmetic operations allows to decide on the applicability of KAM Theorem.

The problem is much more involved when we want to apply KAM Theorem around an arbitrary totally elliptic periodic orbit which is not known analytically. Even if some analytic expression of the orbit is available, the study of the dynamics on the vicinity at the required order can be not feasible analytically. As it is usual, one can restrict the problem to the study of the vicinity of a fixed point of a symplectic map on a suitable Poincaré section in dimension $2n$.

The goal of this paper is to set up a methodology for the rigorous check of the KAM conditions for the symplectic map (see, e.g., [3]).

We give two examples of application. The first one is a simple classical Hamiltonian system with two degrees of freedom and depending on a parameter c. The main feature is that the potential consists only on quartic terms. Changing c the system can be integrable or display large chaotic domains. In these domains one can guess, by numerical computation of iterates of a Poincaré map, that some tiny islands exist. The problem is to show, rigorously, that indeed there are elliptic periodic points of the Poincaré map inside these islands and KAM conditions hold.

The second example concerns the well-known figure eight solution of the general three-body problem with equal masses. See [7] for a proof of the existence of that orbit, found numerically by Moore [18]. This is an example of "choreography" (see [25], where the notion of choreographic solution was introduced, and the references therein), that is, a T-periodic solution of the N-body problem ($N = 3$ in the present case) such that all the bodies move along the same path with time shift T/N between consecutive bodies. This topic for $N = 3$ has been studied by present authors in [10] where, in particular, it was proved

Key words and phrases. Hamiltonian systems, KAM, N-body problem, computer assisted proofs, verified numerics.

the totally elliptic character of the figure eight on fixed energy levels and remaining at the zero level of angular momentum. Using reductions the problem becomes a Hamiltonian with three degrees of freedom. The related Poincaré map is 4D. In [24] it was claimed, based on a non-rigorous high order computation of a normal form, that the KAM condition is satisfied around the figure eight. The computation of the local expansion of the Poincaré map was done by numerical differentiation using multiple precision and optimal step size for the different orders. In the present paper the validity of the KAM condition for the figure eight orbit is established rigorously.

The paper is organised as follows. In the next two sections the examples with 2 and 3 degrees of freedom are presented and several relevant properties of them are proved or mentioned. In particular the reduction of the three-body problem in present case is explicitly carried out, based on [27]. Then the methodology to be applied is explained, introducing the required notation and emphasizing the rigorous aspects of the CAP (Computer Assisted Proofs). Finally the results obtained by applying the methods to both examples are shown.

2. A family of quartic potentials

As a first example we consider a very simple Hamiltonian

$$H = \frac{1}{2}(p_x^2 + p_y^2 + x^4 + cx^2y^2 + y^4),$$

where $c > -2$ is a real parameter. This is a system widely considered as a paradigm of chaotic system for c large in the relations between classical and quantum mechanics, see for instance [4, 8] and references therein. The energy should be positive and, due to the homogeneity, it can be considered equal to a fixed value. We shall consider the level $H = \frac{1}{2}$. Note that for $c \leq -2$ unbounded motion occurs. The system has some obvious symmetries: It is reversible with respect to time and the changes of sign of x and/or y leave the equations invariant. Furthermore, the symplectic change induced by the change of variables $(x, y) \to (u, v) = \frac{1}{\sqrt{2}}(x + y, y - x)$ keeps the form of the Hamiltonian with the parameter c replaced by $\hat{c} = \dfrac{12 - 2c}{2 + c}$, after a scaling to normalise the coefficients to x^4 and y^4 to 1. Obviously the map $c \to \hat{c}$ is an involution having $c = 2$ as fixed point. It can be written also as $\hat{c} + 2 = \dfrac{16}{c + 2}$. When c ranges in $(-2, \infty)$ increasing its value, the parameter $\hat{c}$ ranges in the same interval but decreasing.

It is immediate to check that the planes (x, p_x), (y, p_y), $(x = y, p_x = p_y)$ and $(x = -y,\ p_x = -p_y)$ are invariant and, for the last two, modulo the change $c \leftrightarrow \hat{c}$, we have the same phase portrait than for the first two.

The first question to be addressed is the integrability of the Hamiltonian. To this end we observe that $H = T + V$ is a classical Hamiltonian and V is homogeneous of degree $k = 4$. We specialize to this degree of homogeneity a theorem due to Morales-Ramis [20]

Theorem 1. *Assume $H = T + V = \frac{1}{2}(p_1^2 + \ldots + p_n^2) + V(x_1, \ldots, x_n)$ where V is homogeneous of degree 4. Let $z = (z_1, \ldots, z_n)$ be a solution of $z = \nabla V(z)$ and let $\lambda_1, \ldots, \lambda_n$ be the eigenvalues of Hess $V(z)$. Then, if H is completely integrable with meromorphic first integrals, the values of λ_i must be equal to numbers of the form $2m^2 - m, 2m^2 + \frac{4}{3}m + \frac{7}{72}$ or $2m^2 + 2m + \frac{3}{8}$ for $m \in \mathbb{Z}$.*

Corollary 1. *The Hamiltonian H is only integrable for $c = 0, 2, 6$.*

Proof. Beyond the trivial eigenvalue $\lambda_1 = 3$, due to the homogeneity, one has $\lambda_2 = c/2$, which should be of one of the forms above. Also $\hat{c}/2$ should be of one of these forms. This reduces the possible values of c to $0, 2, 6$. On the other hand the case $c = 0$ is obviously separable and it is also $\hat{c} = 0$ which corresponds to $c = 6$. Finally in the case $c = \hat{c} = 2$ the symplectic change $x = r\sin\varphi$, $y = r\cos\varphi$, $p_x = p_\varphi\cos\varphi/r + p_r\sin\varphi$, $p_y = -p_\varphi\sin\varphi/r + p_r\cos\varphi$ converts the Hamiltonian to $H = \frac{1}{2}\left(p_\varphi^2/r^2 + p_r^2 + r^4\right)$, reducible to 1 degree of freedom. □

See Figure 1 for an illustration of the phase portrait of $\mathcal{P}$ for values of c close to the integrable cases. In the left (resp. right) column the value of c is smaller (resp. larger) than the integrable one. The plots allow to identify easily the bifurcations which occur at the integrable cases.

To understand the dynamics of H as a function of c it is useful to consider the Poincaré section Σ through $y = 0, p_y > 0$, defined for $p_x^2 + x^4 < 1$. The boundary of that domain is a periodic orbit on the invariant plane $y = p_y = 0$. The initial data $x = p_x = 0$ give rise to a periodic orbit $y = y(t)$, sitting on the (y, p_y) plane, which corresponds to a fixed point of the Poincaré map $\mathcal{P}$. The normal

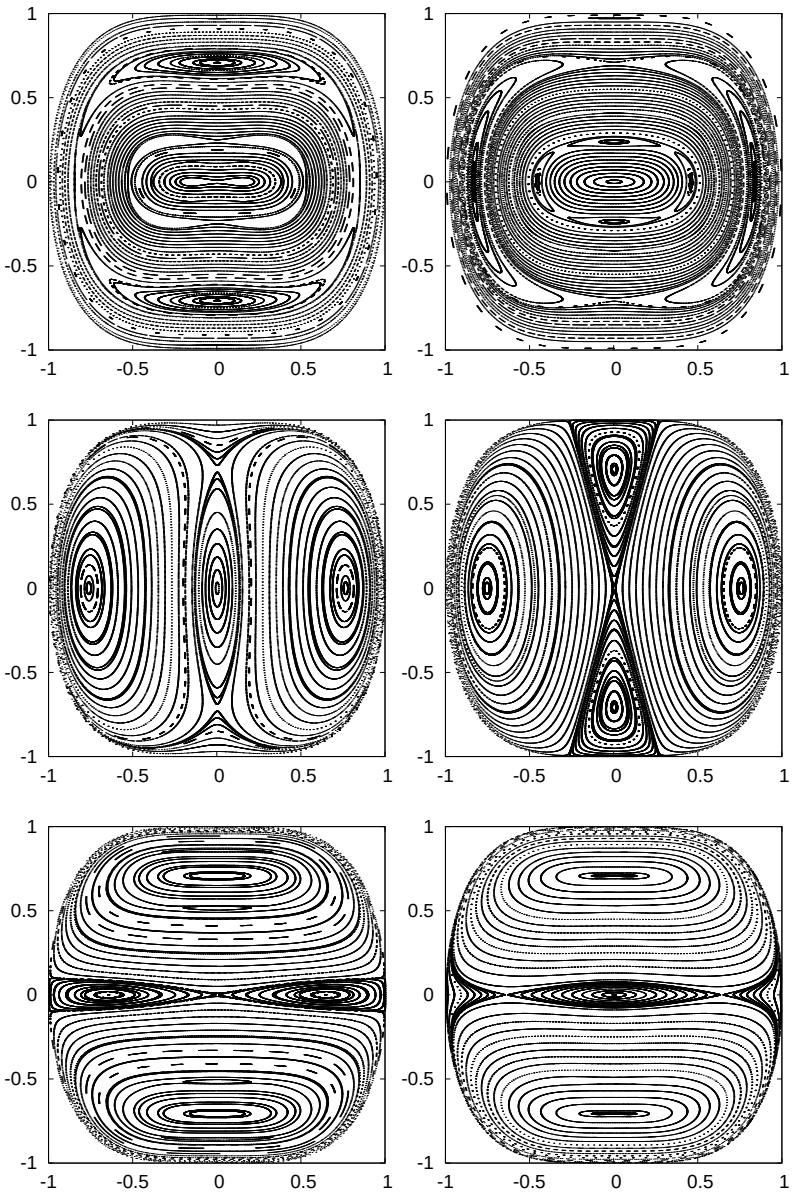

FIGURE 1. Phase portrait on Σ, the Poincaré section $y = 0$, close to the integrable cases. Left column from top to bottom: $c = -0.1, 1.9, 5.9$. Right column $c = 0.1, 2.1, 5.9$. The variables displayed are (x, p_x).

variational equations $\xi' = \eta, \eta' = -cy(t)^2\xi$ give the linear stability of $(0, 0)$. It is easy to check that the trace of $D\mathcal{P}$ at the origin decreases from $+\infty$ to 2 for $c < 0$ and then, for increasing c, it oscillates between -2 and 6. In particular it takes the value $+2$ for $c = c_k = k(k + 1), k \in \mathbb{N}$. For the values $c = (k - 1/2)(k + 1/2)$ it takes, alternatively, the values $+6$ and -2 for k even and odd, respectively. See Figure 2 for an illustration of the behavior of the trace. The set of values of c for which $|\mathrm{Tr}| < 2$ in the union of the intervals $(c_0, c_1) \cup (c_2, c_3) \cup \ldots$, where one has linear stability. The first linear stability intervals are $(0, 2)$, $(6, 12)$, $(20, 30), \ldots$. It is also clear that the periodic orbit at the boundary of Σ has the same stability properties as the orbit we have just discussed.

In a similar way one can consider the initial conditions $x = 0$, $p_x = \sqrt{1/2}$ which correspond to a periodic orbit in $x = y, p_x = p_y$. In that case one can take $x + y = 0$ as Poincaré section. Replacing c by $\hat{c}$ one has a similar result: For $\hat{c} \to -2^+$, which implies $c \to \infty$, this fixed point is unstable for $c > 6$. Stability intervals for $\hat{c}$ are identical to the ones given before for c in the case of the fixed point at the origin. They give rise to intervals which accumulate to -2. The first intervals (in the c parameter) are $(2, 6)$, $(-6/7, 0)$, $(-3/2, -14/11)$, $(-50/29, -18/11)$, $(-42/23)$, $(-66/37)$, etc. We shall

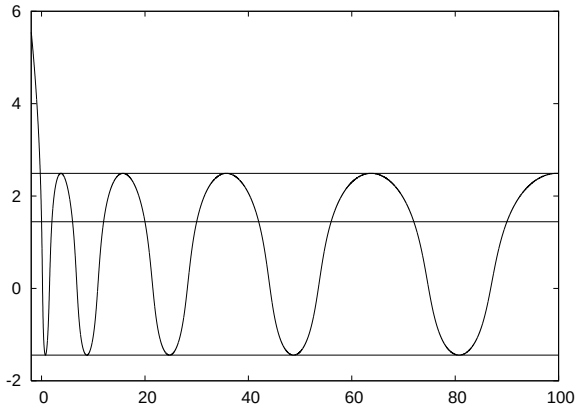

FIGURE 2. Trace of the differential of the Poincaré map $\mathcal{P}$ at the origin as a function of c. On the vertical axis, to prevent from the effect of the large values when $c \to -2^+$, we plot argsinh(Tr) instead of Tr. The horizontal lines correspond to -2, 2 and 6.

refer to these two periodic orbits as the basic ones. Of course, symmetries give rise to similar orbits, like the one through $x = 0$, $p_x = -\sqrt{1/2}$

To see the evolution of the phase space away from the integrable cases we have computed an estimate of the "fraction of chaotic motion" in Σ as a function of c. Due to the symmetries it is enough to do the computations for $x \geq 0$, $p_x \geq 0$. In the domain bounded by $x = 0$, $p_x = 0$ and $p_x^2 + x^4 = 1$ we have selected "pixels" with centre of the form $(i/2000, j/2000), i, j \in \mathbb{N}$ and for each one we have estimated the maximal Lyapunov exponent Λ. In fact we are not interested on the concrete value but rather on whether one can accept $\Lambda = 0$. Symmetry and some other simplifications allow to reduce the computational task. Then the fraction of chaotic motion $\psi(c)$ is estimated as the number of pixels for which one has evidence that $\Lambda > 0$ divided by the total number of pixels in the domain. Several checks have been done using different strategies and maximal number of iterates of the Poincaré map to have reliable information (see, e.g., [23] for details). The results are shown in Figure 3.

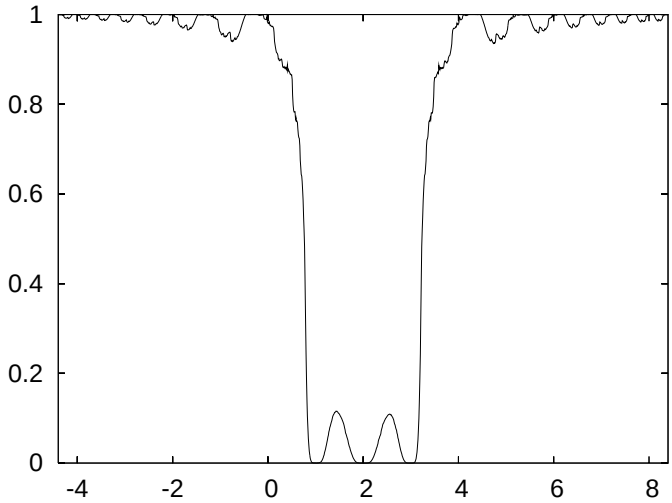

FIGURE 3. Fraction of chaotic dynamics $\psi(c)$ in the Poincaré section Σ as a function of the parameter c. To better see the behavior of the function ψ the variable displayed in the horizontal axis is $d(c) = \log(c + 2)/\log(2)$ instead of c. The three integrable cases $c = 0$, 2, 6 for which $\psi(c) = 0$ are seen on $d = 1$, 2 and 3,respectively.

The interpretation of the figure is clear: close to the integrable cases most of the dynamics is regular. In fact, if c^* is one of the values of c for which one has integrability, the fraction of chaoticity seems to be exponentially small in $|c - c^*|$ for nearby values. Between these values of c the value of $\psi(c)$ is below 0.12. Then, to the left of $c = 0$ and to the right of $c = 6$ there is a quick increase of $\psi(c)$. But at the

ranges in which one of the basic periodic orbits is linearly stable, we can expect the existence of islands, which decrease the measure of the chaotic domain. The oscillations of the decrease are becoming smaller when the limits, either $c \to -2^+$ or $c \to \infty$ are approached.

More concretely, the system away from the range of values of c where it is close to integrable, has a well defined and repetitive structure. To this end we consider the "fraction of integrability" $1 - \psi(c)$. Figure 4 shows it for the values of the parameter c on the right hand side of the domain which contains the close to integrable dynamics. On the left hand side of that domain the plot is symmetrical to the one shown in Figure 4 left. To better see the scaling properties, the horizontal parameter r is an extension of the index k to the real numbers, defined by $r(r+1) = c$. The different "bumps" are quite similar, and the heights scale as $\approx 1/r$. The right part of Figure 4 shows the behavior for $c \in [c_4, c_6]$, which is similar for all the ranges $[c_{2m}, c_{2m+2}], m \geq 2$. At $c = 20$ the central periodic orbit becomes again elliptic (see Figure 2) (remember that the same thing happens for the periodic orbit at the boundary of Σ). A domain of regular motion starts which is reminiscent of the behavior found in many other problems. See, for instance, the reference [26] in the case of the Hénon map. However there are important differences due to the many symmetries of present problem. Anyway the mechanisms to explain the behavior of the plot are the ones explained in [26]. For instance, around $c = 25.6$ the "last" curve surrounding the period 4 islands breaks down and this increases the size of the main chaotic zone.

At $c = 30$ the central periodic orbit becomes unstable by a pitchfork bifurcation and its separatrices display the typical figure eight shape, similar to the example displayed in the central plot in Figure 5. Each part of the figure eight, skipping the invariant curves surrounding the full figure eight separatrix, is really close to the behavior of the Hénon map (except by nonlinear scalings in variables and parameters). The decrease of the regular dynamics in Figure 4 right from $c = 30$ to $c \approx 31.1$ is due to the destruction of the invariant curves surrounding the full figure eight separatrix. Then, at the approximate c values 32.0, 32.5, 33.5, 35.0 and 36.8 the decrease in the fraction is due to the destruction of curves surrounding period 6, 5, 4 and 3 islands and to the period doubling, respectively. It is worth to mention that for the case of period 3 almost no point has regular dynamics. The dynamics in that case, including existence of tiny period 3 islands and other properties, is in perfect agreement with the ones of the Hénon map as studied in [11].

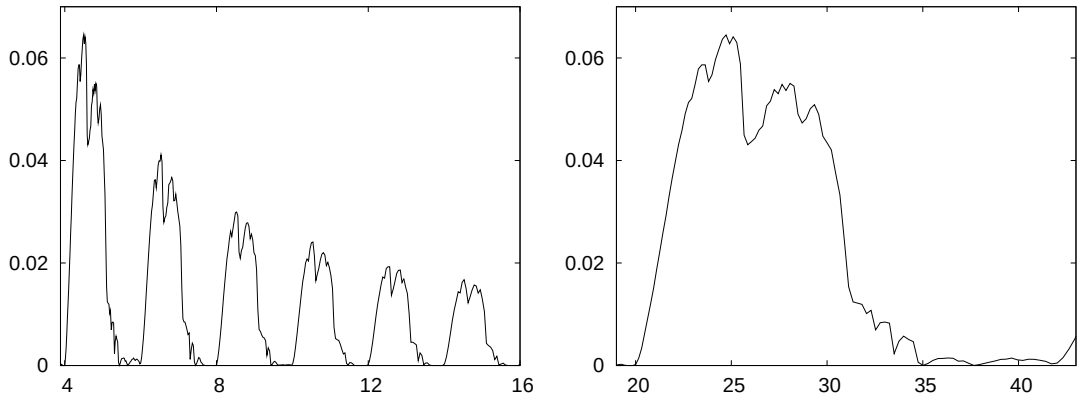

FIGURE 4. Left: The fraction of integrability as a function of r, defined by $r(r+1) = c$. Right: Idem for a range of c containing $[c_4, c_6] = [20, 42]$ using c as horizontal variable.

Our goal is to detect periodic orbits, well inside a chaotic domain, to which we can apply the methodology to be explained to test the KAM conditions. To this end we have selected the value $c = -0.90$ (or, equivalently $\hat{c} = 138/11$), for which the value of ψ is approximately 0.9528. Iterates of the Poincaré map are easily obtained. Using Taylor method at order 30 and a maximal relative truncation error of 10^{-21} they are computed at an average rate of 15,000 iterates per second for that value of c.

The Figure 5 shows a global view of the phase portrait and some details. As this value of c is in one of the instability domains, the periodic orbit through $(0, \sqrt{1/2})$ is unstable, but c is not too far from the left end of one of the stability intervals, at $c = -6/7$. Then the chaotic zone around the figure eight separatrix is still surrounded by invariant curves. Inside that chaotic zone there exist several stable periodic orbits. On the central part of Figure 5 one can see a period 16 orbit. We shall test the KAM conditions for that orbit. An approximate initial condition on Σ is $x = 0$, $p_x = 0.51780665799545$. But

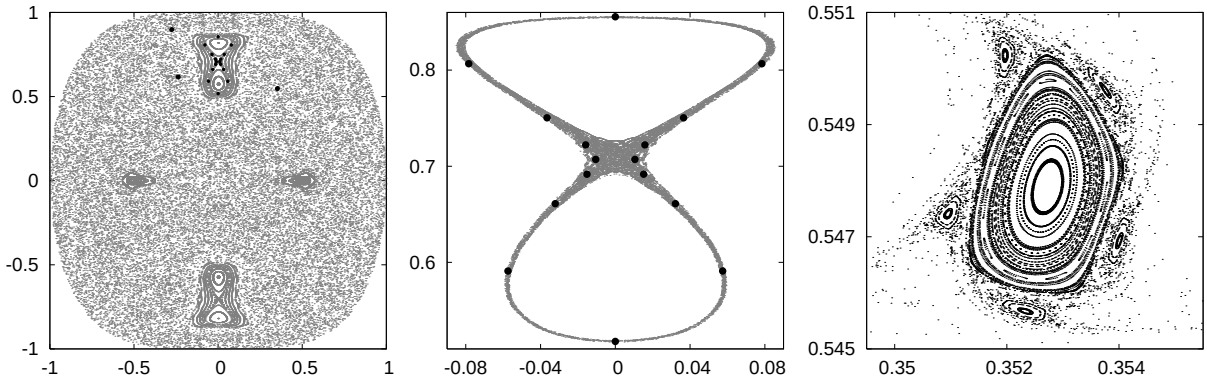

FIGURE 5. Phase portrait on Σ for $c = -0.90$. Left: a global view (in grey) and two periodic orbits (in black). Centre: a magnification of the chaotic zone around the figure eight separatrix associated to the unstable periodic orbit on $(0, \sqrt{1/2})$ and a stable periodic orbit of period 16. Right: The island and some satellite islands near one of the period 3 points, well inside the large chaotic domain.

also a periodic orbit of period 3, far away from that separatrix, deeply inside the chaotic domain, has been found. An approximate initial condition for this orbits is $x = 0.352718557335$, $p_x = 0.547882838499$, and the applicability of KAM theorem for this orbit will also be checked.

We remark that the largest area inside an invariant curve around that period-3 island is of the order of 7×10^{-6}. It is not easy to capture this periodic orbit, but the previous computation of Lyapunov exponents in a grid with small stepsize is of great help.

3. The problem of the KAM stability of the Eight

The figure eight periodic orbit, shown in Figure 6, is a remarkable solution of the planar three-body problem with equal masses [7]. The three bodies move on the plane along the same path in solutions of the form $q(t), q(t + T/3), q(t + 2T/3)$ where T is the period. In [24] a detailed numerical study of this orbit and an extended vicinity of it was done, looking also at the effect of small changes in the masses and the bifurcations that they create. See also [6] for choreographies related to the figure eight, like the satellite and the relative ones. The numerical evidence given in [24] suggested that non only the orbit was linearly stable but also KAM theorem applies around it. The rigorous proof of the linear stability was given in [10] and the proof of the applicability of KAM is studied now.

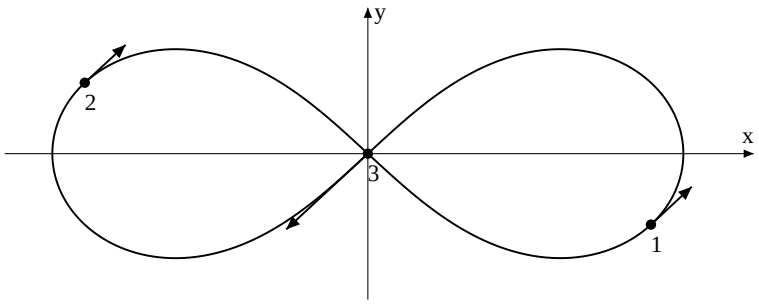

FIGURE 6. The figure eight periodic solution for the planar three-body problem.

The figure eight solution, three nearby partially hyperbolic periodic orbits, as well as several 2D and 3D tori around the eight can be seen in [24]. The orbit has zero total angular momentum and due to the homogeneity of the potential and Kepler's law, one can fix either the level of (negative) energy or the period.

The first step to be done is the reduction of the problem to a three degrees of freedom system. This is a classical result and we follow the exposition that can be found in Whittaker's treatise [27]. For completeness a short account is given below.

3.1. **Reduction of the 3-Body Problem.** We shall assume that the masses are equal to 1. Let $\mathbf{q}_1, \mathbf{q}_2, \mathbf{q}_3$ be the positions of the three bodies in $\mathbb{R}^2$ and $\mathbf{p}_1, \mathbf{p}_2, \mathbf{p}_3$ the corresponding momenta. The Hamiltonian is

$$H = \frac{1}{2}(|\mathbf{p}_1|^2 + |\mathbf{p}_2|^2 + |\mathbf{p}_3|^2) - \frac{1}{|\mathbf{q}_2 - \mathbf{q}_3|} - \frac{1}{|\mathbf{q}_3 - \mathbf{q}_1|} - \frac{1}{|\mathbf{q}_1 - \mathbf{q}_2|}$$

and the angular momentum is $\mathbf{M} = \mathbf{q}_1 \wedge \mathbf{p}_1 + \mathbf{q}_2 \wedge \mathbf{p}_2 + \mathbf{q}_3 \wedge \mathbf{p}_3$.

Let $\mathbf{q}_1', \mathbf{q}_2', \mathbf{q}_3', \mathbf{p}_1', \mathbf{p}_2'$, and $\mathbf{p}_3'$ be new variables introduced by means of the generating function

$$W = (\mathbf{p}_1, \mathbf{q}_1') + (\mathbf{p}_2, \mathbf{q}_2') + (\mathbf{p}_1 + \mathbf{p}_2 + \mathbf{p}_3, \mathbf{q}_3'),$$

where (,) denotes scalar product. We recall that

$$\mathbf{q}_j = \frac{\partial W}{\partial \mathbf{p}_j}, \quad \mathbf{p}_j' = \frac{\partial W}{\partial \mathbf{q}_j'},\ j = 1, 2, 3$$

and, hence, the change gives

$$\mathbf{q}_1 = \mathbf{q}_1' + \mathbf{q}_3',\ \mathbf{q}_2 = \mathbf{q}_2' + \mathbf{q}_3',\ \mathbf{q}_3 = \mathbf{q}_3',\ \mathbf{p}_1 = \mathbf{p}_1',\ \mathbf{p}_2 = \mathbf{p}_2',\ \mathbf{p}_3 = \mathbf{p}_3' - \mathbf{p}_1' - \mathbf{p}_2'.$$

Because of the centre of mass integrals, it is not restrictive to assume $\mathbf{q}_1 + \mathbf{q}_2 + \mathbf{q}_3 = 0, \mathbf{p}_1 + \mathbf{p}_2 + \mathbf{p}_3 = 0$, which amounts to $\mathbf{q}_3' = -(\mathbf{q}_1' + \mathbf{q}_2')/3$ and $\mathbf{p}_3' = 0$, Hence, the new expressions of H and M, skipping the $'$ for simplicity, are

$$H = |\mathbf{p}_1|^2 + |\mathbf{p}_2|^2 + (\mathbf{p}_1, \mathbf{p}_2) - \frac{1}{|\mathbf{q}_1|} - \frac{1}{|\mathbf{q}_2|} - \frac{1}{|\mathbf{q}_1 - \mathbf{q}_2|}, \quad M = \mathbf{q}_1 \wedge \mathbf{p}_1 + \mathbf{q}_2 \wedge \mathbf{p}_2,$$

which reduce the system to 4 degrees of freedom.

Let (q_1, q_2) be the components of $\mathbf{q}_1$, (q_3, q_4) the ones of $\mathbf{q}_2$ and, in a similar way, we define the components of the $\mathbf{p}$ variables. We introduce the generating function

$$W = p_1 q_1' \cos q_4' + p_2 q_1' \sin q_4' + p_3(q_2' \cos q_4' - q_3' \sin q_4') + p_4(q_2' \sin q_4' + q_3' \cos q_4'),$$

which gives raise to the transformation

$$q_1 = q_1' \cos q_4',\ q_2 = q_1' \sin q_4',\ q_3 = q_2' \cos q_4' - q_3' \sin q_4',\ q_4 = q_2' \sin q_4' + q_3' \cos q_4',$$
$$p_1 = p_1' \cos q_4' - ((p_4' - q_2' p_3' + q_3' p_2') \sin q_4')/q_1',$$
$$p_2 = p_1' \sin q_4' + ((p_4' - q_2' p_3' + q_3' p_2') \cos q_4')/q_1',$$
$$p_3 = p_2' \cos q_4' - p_3' \sin q_4',\ p_4 = p_2' \sin q_4' + p_3' \cos q_4'.$$

Skipping again the $'$, one can write the Hamiltonian and angular momentum in the new variables. It turns out that the new q_4 does not appear in H. It is a cyclic variable. Hence, the conjugated variable p_4 is constant. But it is immediate to see that $M = p_4$. We still keep its value in the Hamiltonian, despite in the case of the figure eight $M = 0$, because it plays a role in the "rotating eights" solutions. The final reduced Hamiltonian has the form

$$\begin{aligned} H &= p_1^2 + p_2^2 + p_3^2 + p_1 p_2 - \frac{p_3}{q_1}(q_2 p_3 - q_3 p_2 - p_4) + \frac{1}{q_1^2}(q_2 p_3 - q_3 p_2 - p_4)^2 \\ &\quad - \frac{1}{q_1} - \frac{1}{(q_2^2 + q_3^2)^{1/2}} - \frac{1}{((q_1 - q_2)^2 + q_3^2)^{1/2}}. \end{aligned} \tag{2}$$

The new variables have a simple geometrical meaning. Let us denote the positions of the masses as $m_j, j = 1, 2, 3$ and as $m_i m_j$ the vector from m_i to m_j. Then q_1 is the norm of $m_3 m_1$ and p_1 is the component of the linear momentum of m_1 projected along $m_3 m_1$; q_2 and q_3 are the projections of $m_3 m_2$ along $m_3 m_1$ and orthogonal to it and, in a similar way, p_2 and p_3 are the projections of the linear momentum of m_2; finally q_4 is the angle between the x-axis and $m_3 m_1$. As said, $p_4 = M$.

3.2. **Rotating Eights.** If the angular momentum M goes away from zero, the periodic orbit can be continued. It becomes quasi-periodic with two basic frequencies, which will produce a periodic orbit if the ratio of frequencies is rational. But it can be seen again as a periodic solution, even as a choreography, using a rotating frame, a fact noticed by M. Hénon [9] who also found that the continuation leads to collision orbits. Due to the symmetries of the problem it is enough to consider M increasing to positive values. For most of these "rotating eights" we can apply the same algorithm as for the Eight. The Figure 7 shows the values of $\alpha_1 < \alpha_2$ such that the eigenvalues of the Poincaré map associated to the rotating eight are $\exp(\pm 2\pi \mathrm{i}\, \alpha_1)$, $\exp(\pm 2\pi \mathrm{i}\, \alpha_2)$, as a function of M. The monotonically decreasing line gives the minimal distance between the bodies along the orbit, an evidence of a nearby collision. The plot changes at $M = M_{pd} \approx 0.4467$, when $\alpha_2 = 1/2$, and then the orbit loses stability with the appearition of a period

doubling bifurcation. For $M > M_{pd}$ we plot the logarithm of the modulus of the dominant eigenvalue (divided by 2 to fit in the plot). Low order resonances $k_1\alpha_1 + k_2\alpha_2 \in \mathbb{N}$ with $|k_1| + |k_2| \leq 4$ are easy to detect for different values of M. For them additional terms will appear in the normal form making our arguments not valid in these cases. Therefore, as an example, we have selected two values of the angular momentum, $M_1 = 0.0048828125$ and $M_2 = 0.1484375$, that are far enough from resonances. A non-rigorous exploration of orbits close to the rotating eights for $|M| < M_{pd}$ gives evidence that for most of them the numerical simulation suggests the existence of tori, but for some resonances they seem to be destroyed.

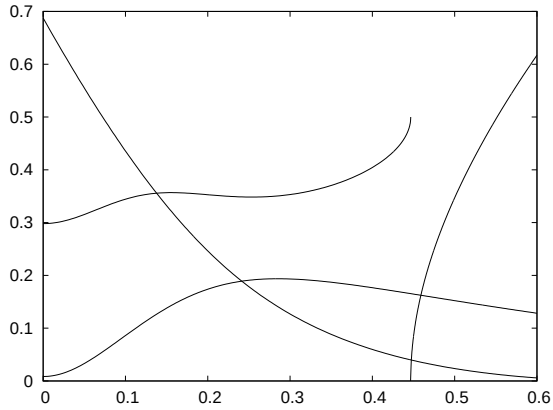

FIGURE 7. Arguments α_1, α_2 of the eigenvalues $\exp(\pm 2\pi \mathrm{i}\,\alpha_1), \exp(\pm 2\pi \mathrm{i}\,\alpha_2)$ corresponding to the rotating Eights solutions for a range of values of angular momentum M. When α_2 reaches the value $1/2$ for $M = M_{pd} \approx 0.4467$ a period doubling is produced and the orbit becomes unstable with a dominant eigenvalue $\lambda < -1$. From that value on, instead of α_2 we plot $\log(|\lambda|)/2$. The line which decreases monotonically shows the minimal distance between the bodies along the rotating Eight.

Initially the rotating eights, in coordinates which rotate with the suitable angular velocity, look similar to the orbit shown if Figure 6, but the left and right hand side lobes are no longer symmetric. Later on the orbits in the rotating frame can develop extra loops. As an example Figure 8 shows the solution obtained for $M \approx 0.4493$, shortly after the orbits become unstable. The value of M has been selected so that in the fixed frame (middle panel) the orbit is also periodic. On the left panel the orbit is shown in a rotating frame. At some moment, as displayed, one of the bodies is on the rightmost point on the path, on the small loop on the right, and the other two are symmetrical w.r.t. the horizontal axis, on the large loop on the left. When the bodies move they pass very close to collision on the tiny central lobe. The right panel shows a 3D projection, on the variables (q_1, q_2, p_1), of what is seen in the Poincaré section. The large dot represents the periodic orbit. An initial point, taken by adding 10^{-9} to q_1, is iterated under the Poincaré map. The points are scattered close to the "separatrix" associated to the unstable/stable directions. Of course, these 1D manifolds do not coincide, but the splitting must be expected to be exponentially small in $M - M_{pd}$.

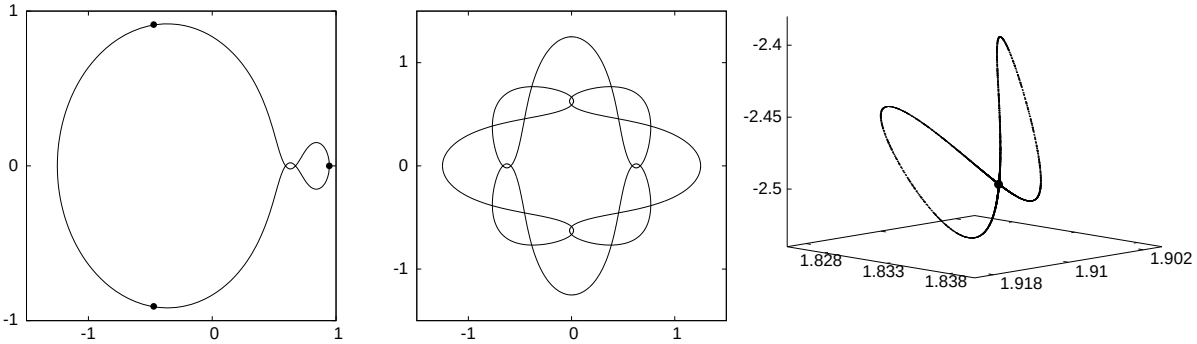

FIGURE 8. A rotating eight for $M \approx 0.4493$, already on the linear instability domain. See the text for a detailed explanation.

4. Preliminaries and the algorithm

Before going into details we want to emphasize that the algorithm presented in this paper is **rigorous**. By rigorous we mean that during all the computations we take into account and bound all possible errors. In this way we get not the exact values but verified estimates of the computed quantities. Therefore the theorems that we apply have assumptions of a special kind (i.e. inequalities, inclusions etc.) that can be checked using those estimates. As a result we obtain a computer assisted method to have proofs of the existence and the KAM stability of periodic orbits for Hamiltonian systems that has full mathematical rigor. In theory all calculations could be done by paper and pencil, but in practice the number of operations, even if they are very basic and trivial, exceeds human resources.

4.1. **Interval arithmetics.** As the precision of the computer is finite we use an interval arithmetic to take care of the round-off errors. All floating point operations are replaced by the corresponding operations on closed intervals such that we always obtain some representable superset of the true result. This is also extended to all elementary functions.

For the rest of the paper, following [13], we use boldface to denote intervals and objects with interval coefficients. For those objects we use the names *interval vector* (or *box*), *interval matrix* etc. to stress their interval nature. For a set S by $\operatorname{hull} S$ we denote the interval hull of S i.e. the smallest product of intervals containing S. For an interval $\boldsymbol{a} = [\underline{a}, \overline{a}]$ we define its diameter by $\operatorname{diam} \boldsymbol{a} := \overline{a} - \underline{a}$. We define *the diameter of a box* $\boldsymbol{x} = (\boldsymbol{x}_1, \boldsymbol{x}_2, \dots, \boldsymbol{x}_n)$ as a maximal diameter of its components i.e. $\operatorname{diam}(\boldsymbol{x}) = \max\{\operatorname{diam} x_k | k = 1, \dots, n\}$.

4.2. **The rigorous computation of Taylor expansions of Poincaré maps.** To rigorously integrate ODEs and to obtain verified enclosures for the partial derivatives with respect to the initial conditions we use $\mathcal{C}^1$-Lohner [29] and $\mathcal{C}^r$-Lohner [28] algorithms implemented in the CAPD library [5]. Those algorithms are based on the Taylor integrator and set representations proposed by Lohner. For some set of data (say the box $\boldsymbol{x}$) and time step h the $\mathcal{C}^r$-Lohner algorithm produces rigorous enclosures for the solution $\varphi(x, h)$ of the ODE and its derivatives $\frac{\partial^{|\alpha|}\varphi(x,h)}{\partial x^\alpha}$ for all initial points $x \in \boldsymbol{x}$ and all multiindices $|\alpha| \leq r$. The specialized $\mathcal{C}^1$-Lohner algorithm is able to compute only first order derivatives.

The "naive" representation of the derivatives as a table of interval vectors leads to a huge overestimation due to the "wrapping effect" (see [19, 16]). Hence, internally during the integration, for each multiindex α the corresponding vector $v = \frac{\partial^{|\alpha|}\varphi(x,h)}{\partial x^\alpha}$ is stored in one of the Lohner representations [16]. For that reason even $\mathcal{C}^0$ algorithms need $\mathcal{C}^1$ information to properly set coordinates to suppress the "wrapping" error. In the current implementation to store derivatives we use doubletons

$$v = x_0 + Cr_0 + Br,$$

where x_0 is a point vector (the centre), C and B are matrices of "good" coordinates (usually C is close to the Jacobian matrix and B is its orthogonalization), r_0 represents the initial size of vector v and r stores all computational errors.

To compute all the derivatives up to order r for an n dimensional ODE we need to solve $n\binom{n+r}{n}$ equations. If they would be solved directly it would lead to the integration in a high dimensional space and is usually inefficient (most of the rigorous solvers internally need C^1 information that squares the dimension). The $\mathcal{C}^r$-Lohner algorithm makes use of the special structure of the variational equations to avoid this and as a result it can bound derivatives to an arbitrary order r in an efficient way.

On top of those rigorous ODE solvers the CAPD library implements algorithms to rigorously compute Poincaré maps and their derivatives with respect to the initial conditions for an affine sections (for details see [29, 28]).

4.3. **Notation and definitions related to Hamiltonian systems.** We denote by J the Poisson matrix

$$J = \begin{pmatrix} 0 & I_n \\ -I_n & 0 \end{pmatrix},$$

where I_n denote the n dimensional identity matrix. The *Poisson bracket* of functions $f, g : \mathbb{R}^{2n} \supset M \mapsto \mathbb{R}$ is a new function $\{f, g\} := (\nabla f)^T J \nabla g$.

By $\mathbb{N}^+$ we denote set of all positive integers i.e. $\mathbb{N}^+ = \{1, 2, \dots\}$ and we define $\mathbb{N} := \{0\} \cup \mathbb{N}^+$. An element of $\mathbb{N}^n$ will be called a *multiindex*. For a multiindex $k = (k_1, k_2, \dots, k_n)$ and a vector $v = (v_1, v_2, \dots, v_n)$ we define

- $|k| = \sum_{j=1}^n |k_j|$,

- $v^k = v_1^{k_1} v_2^{k_2} \dots v_n^{k_n}$

A vector $(\lambda_1, \lambda_2, \dots, \lambda_n) \in \mathbb{C}^n$ satisfies the non-resonant condition up to order r if for all multiindices $k = (k_1, k_2, \dots, k_n)$ such that $1 < |k| \leq r$ and all $j \in \{1, 2, ..., n\}$ we have

$$\lambda_j \neq \lambda^k. \tag{3}$$

4.4. **The algorithm.** For a given Hamiltonian system (1) we assume that we have an approximate initial condition x_0 of a periodic orbit and a Poincaré section Σ that contains x_0. For fixed level of energy $h \approx H(x_0)$ the Poincaré map defines a symplectic map

$$\mathcal{P} : \Sigma \mapsto \Sigma.$$

We will use $x = (q, p) \in \mathbb{R}^n \times \mathbb{R}^n$ to denote local canonically conjugated variables. Let $\tilde{x}_0$ correspond to x_0 in these variables.

In this setting to prove existence and KAM stability of a periodic orbit given by approximate initial conditions x_0 it is enough to prove for some $k \in \mathbb{N}^+$ the existence and KAM stability of the unique fixed point of $\mathcal{P}^k$ in some small neighbourhood of $\tilde{x}_0$. The algorithm consists of the following steps:

(1) Proof of the existence of the unique fixed point (a periodic orbit).
    Rigorous estimates of initial conditions.
(2) Proof of the linear stability.
(3) Computation of a rigorous Birkhoff normal form.
(4) Checking an appropriate non-degeneracy condition.

The details for each step will be given in the following subsections.

4.5. **Proof of the existence.** In the first step of the algorithm we prove the existence of an unique periodic orbit close to x_0 and obtain rigorous bounds for its initial conditions. Therefore the preliminary step is to reduce the Hamiltonian system (1) by suitable symplectic transformations so that for a given energy level the periodic orbit is isolated. Section 3 contains a (very classical) example showing how it was done in the case of the 3-body problem.

For a proof we take a box $\boldsymbol{x} \subset \mathbb{R}^{2n}$ with centre in $\tilde{x}_0$, and compute rigorous estimates of the interval Newton operator

$$N(\tilde{x}_0, \boldsymbol{x}, F) = \tilde{x}_0 - \text{hull}(DF(\boldsymbol{x}))^{-1} F(\tilde{x}_0)$$

for $F(x) = \mathcal{P}^k(x) - x$. If we succeed to verify that $N(\tilde{x}_0, \boldsymbol{x}, F) \subset \boldsymbol{x}$ then the interval Newton theorem [1, 22] ensures that inside $\boldsymbol{x}$ there exists a unique k-periodic point of $\mathcal{P}$. Instead of Newton method one can also use the interval Krawczyk method [15, 12] which do not requires the whole interval matrix $\text{hull}(DF(\boldsymbol{x}))$ to be invertible.

Remark 1. *The problem of proving the existence of zeros of F when, as in present case, involves the computation of $\mathcal{P}^k(\boldsymbol{x})$ is well suited for the use of the parallel shooting method. In our implementation we make use of it to improve precision and to speed up computations.*

Remark 2. *One can improve rigorous estimates of the initial condition of the periodic point by further iteration of the interval Newton or Krawczyk operator.*

4.6. **Proof of linear stability.** Current step goal is to prove that all the eigenvalues $(\lambda_1, \lambda_2, \dots, \lambda_{2n})$ of the differential of the iterated Poincaré map $DP = \frac{\partial \mathcal{P}^k(\hat{x})}{\partial x}$, where $\hat{x}$ is a k periodic point of $\mathcal{P}$, lie on the unit circle. We want also to obtain rigorous estimates $\boldsymbol{\lambda_j}$ such that $\lambda_j \in \boldsymbol{\lambda_j}$ for $j = 1, \dots, 2n$.

The point $\hat{x}$ is not known exactly, but from the previous step we have rigorous estimates $\boldsymbol{x}$ of it. From estimates $\boldsymbol{DP} = \frac{\partial \mathcal{P}^k(\boldsymbol{x})}{\partial x}$ using e.g. verified root finding methods applied to the characteristic polynomial one can obtain estimates of the eigenvalues. Because those estimates are given by some boxes, part of them are out of the unit circle. But still the proof of linear stability is possible due to the fact that our system is Hamiltonian.

Lemma 1. *Let $A \in \mathbb{R}^{2n \times 2n}$ be a symplectic matrix with eigenvalues $(\lambda_1, \dots, \lambda_{2n})$, and let $\boldsymbol{\lambda_j}$ be boxes such that $\lambda_j \in \boldsymbol{\lambda_j}$ for $j = 1, \dots, 2n$. If the following holds*

(A1) $0 \notin \text{Im}\,(\boldsymbol{\lambda_j})$ *for* $j = 1, \dots, 2n$
(A2) $(\boldsymbol{\lambda_j}^{-1} \cap \bar{\boldsymbol{\lambda}}_{\boldsymbol{k}} \neq \emptyset) \implies j = k,$

then all eigenvalues of A are distinct and lie on the unit circle.

Proof: The matrix A is symplectic, hence if λ is an eigenvalue of A then also $\lambda_j = \lambda^{-1}$ and $\lambda_k = \bar{\lambda}$ are eigenvalues. But then assumptions (A1) and (A2) ensure that $\lambda^{-1} = \bar{\lambda}$ and hence $\|\lambda\| = 1$. From (A2) we have also that all eigenvalues are distinct. □

This general method requires sharp bounds for the eigenvalues. This can be a not so easy task in general. Another possibility is to translate constraints to the characteristic polynomial. In this case one proves first that the eigenvalues are on the unit circle and then rigorous enclosures $\boldsymbol{\lambda_i}$ are obtained using this fact (see for example [10]).

4.7. **Computation of Birkhoff normal form.** The literature on how to compute Birkhoff normal form is very rich. There are also general software packages that can do it in a non rigorous way. Here we want to explain how to make this process rigorous. All the computations are done using interval arithmetics in the way that at the end the normal form will have interval coefficients that contain the exact values.

Let $T(x) = (\sum_{k\in\mathbb{N}^{2n}} c_{1,k}x^k, \dots, \sum_{k\in\mathbb{N}^{2n}} c_{2n,k}x^k)$ be the Taylor series of an analytic symplectic map around a totally elliptic fixed point and let $(\lambda_1, \dots, \lambda_n, \bar{\lambda}_1, \dots, \bar{\lambda}_n)$ be the eigenvalues of the linear part of T. Then for $j \in \{1, 2, ..., 2n\}$ and a multiindex k such that $k_j = k_{j\pm n} + 1$ and $k_m = k_{m+n}$ for $m \neq j$ the condition (3) is not satisfied and a resonance occurs. We call it an *unavoidable resonance* and we say that the term $c_{j,k}x^k$ corresponds to that resonance. A Taylor series T is said to be *non-resonant* if only unavoidable resonances are present.

The goal of this section is to make a symplectic change of variables such that in the new variables the Taylor series T up to a given order r reads

$$z \mapsto \Lambda z + T_r(z),$$

where Λ is a diagonal matrix, $\Lambda = diag(\lambda_1, \dots, \lambda_n, \bar{\lambda}_1, \dots, \bar{\lambda}_n)$, and $T_r(z)$ contains only terms corresponding to unavoidable resonances. This is the so called *non-resonant Birkhoff normal form*. In what follows we present an algorithm that computes the non-resonant Birkhoff normal form up to order 3, but it can be easily extended to any given order.

First, using C^r-Lohner algorithm [28] we compute rigorous enclosures of the coefficients of the Taylor expansion of $\mathcal{P}^k$ up to order 3 for all points in $\boldsymbol{x}$ (an estimate of the fixed point). As a result we obtain a symplectic map (up to order 3)

$$T : (q_1, \dots, q_n, p_1, \dots, p_n) \to (\hat{q_1}, \dots, \hat{q_n}, \hat{p_1}, \dots, \hat{p_n}).$$

We recall that from the previous step we know that the eigenvalues $\lambda = (\lambda_1, \dots, \lambda_{2n})$ of the linear part of T lie on the unit circle.

As a second step we pass the linear part to a diagonal form

$$\Lambda = \mathrm{diag}(\lambda_1, \lambda_2, \dots, \lambda_{2n}).$$

To this end we use the linear change, B, given by a matrix formed by eigenvectors corresponding to the above eigenvalues. As we do not know the exact eigenvalues, the estimate of an eigenvector corresponding to λ_i, has to be valid for all $\lambda_i \in \boldsymbol{\lambda_i}$. To ensure that B is symplectic we use the following lemma and replace the previous eigenvectors by suitable multiples of them.

Lemma 2. *Let $A \in \mathbb{R}^{2n\times 2n}$ be a symplectic matrix with eigenvalues $(\lambda_1, ..., \lambda_n, \lambda_{n+1} = \bar{\lambda}_1, \dots, \lambda_{2n} = \bar{\lambda}_n)$ such that $|\lambda_i| = 1$ and $\lambda_i \neq \lambda_j$ for $i, j = 1, \dots, 2n$ and $i \neq j$. Let $(e_1, \dots, e_{2n})$ be corresponding eigenvectors. If $e_i^T J e_{i+n} = 1$ for $i = 1, \dots, n$ then the eigenbasis $B = (e_1, e_2, \dots, e_{2n})$ is symplectic.*

Proof: To be symplectic matrix B needs to satisfy $B^T JB = \{e_i^T J e_j\} = J$. Due to antisymmetry we can assume that $i \leq j$. For $j = i + n$ we already have that $e_i^T J e_{i+n} = 1$. For $j \neq i + n$ we have $\lambda_i\lambda_j \neq 1$ and therefore $e_i^T J e_j = e_i^T A^T J A e_j = \lambda_i\lambda_j e_i^T J e_j = 0$. □

In our implementation initially e_i and e_{i+n} are complex conjugate vectors, therefore $e_i^T J e_{i+n} = \mathrm{i}\, c$ for some $c \in \mathbb{R}$. We want to scale those vectors to get $e_i^T J e_{i+n} = 1$ and additionally $e_i = \mathrm{i}\,\bar{e}_{i+n}$. This is possible only if $c < 0$. Therefore if $c > 0$ we simply interchange the indices of corresponding eigenvalues and eigenvectors. Finally we set

$$e_i \leftarrow \tfrac{e_i}{\sqrt{-c}}, \qquad e_{i+n} \leftarrow \tfrac{e_{i+n}}{-\mathrm{i}\sqrt{-c}}.$$

Let $u = (u_1, \dots, u_{2n})$ be the new coordinates in this basis. The above scaling implies that $u_i = \mathrm{i}\,\bar{u}_{i+n}$ for $i = 1, \dots, n$. The final form of the symplectic transformation up to order 3, before starting the normal form computation, is

$$S = B^{-1} \circ T \circ B : u \to \Lambda u + S_2 + S_3,$$

where S_2 and S_3 denote quadratic and cubic terms of $S(u)$ respectively.

Let us denote as $U = (U_1, \ldots, U_{2n})$ the coordinates of the normal form. We achieve a normal form in two steps, by cancelling first all the terms of degree two in S and then the terms of degree three, except the unavoidable resonances. For the first step we should select, in principle, a transformation of the form

$$u = N_1(U) = U + Q(U),$$

where $Q(U) = (Q_1, \ldots, Q_{2n})^T$ are quadratic terms. To cancel the terms of degree two in S we require that

$$S \circ N_1 = N_1 \circ \Lambda \tag{4}$$

holds up to degree two. Let us express this in coordinates. Assume that the quadratic terms of S and N_1 are written, respectively, as

$$(S_2)_j = \sum_{|k|=2} c_{j,k} u^k, \qquad Q_j = \sum_{|k|=2} d_{j,k} U^k, \qquad \text{for } j = 1, ..., 2n,$$

where k is a multiindex. The condition (4) allows to obtain

$$d_{i,k} = \frac{c_{i,k}}{\lambda_i - \lambda^k}$$

for all the required indices i, k. If there are no resonances of order 2, then all denominators are different from zero. We ensure this using rigorous estimates $\boldsymbol{\lambda}_i$.

However, the map N_1, as it was introduced, is not a symplectic map. Its differential satisfies the symplecticity conditions only to order 1 in U and we need additional cubic terms to satisfy them to order 2. This suggests to define the symplectic transformation as the time-1 map of some Hamiltonian W

$$u = N(U) = \varphi^W_{t=1}(U).$$

To determine W we require

$$\frac{\partial W}{\partial U_{j+n}} = Q_j, \quad -\frac{\partial W}{\partial U_j} = Q_{j+n}, \quad \text{for } j = 1, \ldots, n$$

As the difference between the map and the identity starts with quadratic terms, the Hamiltonian starts with cubic terms. Then the time-1 map adds terms of degree 3 to the initial ones. Finally we obtain the components of $N(U)$ as

$$(N(U))|_j = U_j + Q_j + \frac{1}{2}\{Q_j, W\},$$

where $\{\ ,\ \}$ denotes the Poisson bracket. This produces the normal form to order two as

$$S : U \mapsto \Lambda U + S_3(U),$$

where $S_3(U)$ are the cubic terms.

The last step is to remove all cubic terms except those corresponding to unavoidable resonances. We know that there exists a symplectic, near the identity transformation that will cancel the non-resonant cubic terms leaving the resonant terms unchanged. Hence we can simply set to zero all terms in $S_3(U)$ for which we are able to verify non-resonant condition.

Finally we obtain the normal form to order three (we use z as a new variables)

$$S : z \mapsto \Lambda z + T_3(z),$$

where $T_3(z)$ are the cubic terms corresponding to unavoidable resonances.

It remains to check the non-degeneracy condition which allows to apply KAM theorem. This is now easy and will be done directly on the examples.

5. Results

In this section we present the results of the application of the algorithm to the examples introduced in sections 2 and 3. The computed values are often very thin intervals with lower and upper bound having many common leading digits. To increase readability when printing intervals we put first those common digits and then the remaining digits of lower and upper bound as subscript and superscript correspondingly, e.g.

$$\begin{aligned} 123.456789^{5678}_{1234} &= [123.4567891234, 123.4567895678], \\ -123.456789^{5678}_{1234} &= [-123.4567895678, -123.4567891234], \\ ^{0.0000000001}_{-0.0000000001} &= [-0.0000000001, 0.0000000001]. \end{aligned}$$

period	3	16
precision	double (52 bits)	multiprecision (100 bits)
$\boldsymbol{x}$	$\begin{pmatrix} 0.352718557333^{67754}_{27137} \\ 0.54788283 8^{5020712}_{4949869} \end{pmatrix}$	$\begin{pmatrix} {}^{+0.0000000000000001}_{-0.0000000000000001} \\ 0.5178066579954573^{4}_{3} \end{pmatrix}$
$\mathrm{diam}(\boldsymbol{x})$	$7 \cdot 10^{-12}$	10^{-23}
$\boldsymbol{\lambda_1}, \boldsymbol{\lambda_2}$	$0.539^{6}_{4} + \mathrm{i}\, 0.8419 8^{7}_{4}$	$-0.9323905 0^{5}_{4} \pm \mathrm{i}\, 0.3614525 5^{3}_{2}$
$\boldsymbol{c_1}$	$89^{315.580}_{149.071} - \mathrm{i}\, 139^{345.393}_{180.278}$	$137393^{1.069}_{0.985} - \mathrm{i}\, 532621.^{177}_{066}$
$\boldsymbol{c_2}$	$-89^{307.807}_{156.837} - \mathrm{i}\, 139^{337.719}_{187.959}$	$-137393^{1.065}_{0.988} - \mathrm{i}\, 532621.^{173}_{070}$
$\boldsymbol{d}$	$263^{42.269}_{05.594} + \mathrm{i}\, {}^{+18.283}_{-18.281}$	$-234523.9^{71}_{51} + \mathrm{i}\, {}^{+0.011}_{-0.011}$

TABLE 1. Rigorous estimates of the initial condition $\boldsymbol{x}$, eigenvalues $\boldsymbol{\lambda_1}, \boldsymbol{\lambda_2}$, coefficients of normal form $\boldsymbol{c_1}, \boldsymbol{c_2}$ and torsion $\boldsymbol{d}$ for the proof of the KAM stability of orbits of period 3 and 16 for the quartic potential.

To be rigorous the presented intervals are rounded outwards, e.g the interval $[10^{-21}, 10^{-18}]$ when rounded to 3 decimal places reads 0.00^{1}_{0}. That sometimes can suggests that consecutive interval operations are not correct but in fact they are performed with much higher precision than the one displayed, e.g. the result of $1000 \cdot 0.00^{1}_{0}$ can still be equal to 0.00^{1}_{0}.

5.1. **The quartic potential example.** For an approximated initial condition as given in section 2 we carry out the algorithm described in section 4. The computed values are displayed in the Table 1. From the first step of the algorithm we obtain a rigorous estimate of the initial condition: $\boldsymbol{x}$. We use them to get enclosures for the eigenvalues: $\boldsymbol{\lambda_1}$ and $\boldsymbol{\lambda_2}$. The Birkhoff normal form of the third and the sixteenth iterate of the Poincaré map, respectively, computed at the fixed point $x \in \boldsymbol{x}$ in both cases is proved to be

$$\begin{pmatrix} z_1 \\ z_2 \end{pmatrix} \mapsto \begin{pmatrix} \lambda_1 z_1 + c_1 z_1^2 z_2 \\ \lambda_2 z_2 + c_2 z_1 z_2^2 \end{pmatrix} \tag{5}$$

for some $\lambda_j \in \boldsymbol{\lambda_j}$ and $c_j \in \boldsymbol{c_j}$ for $j = 1, 2$. It is enough to work only with the first equation, because $z_1 = \mathrm{i}\, \bar{z}_2$,. Hence the map (up to order 3) reads

$$z_1 \mapsto z_1 \exp(2\pi \mathrm{i}\, (\alpha + d|z_1|^2)) \tag{6}$$

where $\lambda_1 = \exp(2\pi \mathrm{i} \alpha)$ and $d = \frac{c_1}{2\pi\lambda_1}$. Finally, for the twist map (6) if d (the torsion, or twist coefficient in that case) is different from zero then the fixed point is KAM stable (see [3, 21]). The computed rigorous bounds $\boldsymbol{d}$, shown in Table 1, verify that d is not zero for both orbits. Therefore they are KAM stable.

The proof of the existence of the period 16 orbit using double precision did not succeed, and we were forced to use multiprecision interval arithmetic and Taylor method of higher order. This increases in a significant way the computational time.

5.2. **The figure eight orbit.** We start with the coordinate system introduced in section 3 in which the Hamiltonian of the planar 3-body problem has the form (2). The variables are $(q_1, q_2, q_3, p_1, p_2, p_3)$. For the figure eight orbit and nearby orbits we select as Poincaré section the passage through $q_3 = 0$, that is, when the three bodies are aligned. We recall that this collinear passage happens 6 times in a full revolution. Then, given q_1, q_2, p_1 and p_2 and the value of the energy $H = h$ we can determine $p_3 > 0$. The Poincaré map defines a symplectic 4D map on the fixed level of energy and $M = 0$. Local variables which are canonically conjugate are q_1, q_2, p_1, p_2.

Rough initial conditions in these variables if we start when the bodies are aligned, on the x axis, with m_1 to the right and m_2 at the center, are

$$q_1 = 1.9909837697297968,\ q_2 = 0.9954918848648984,\ q_3 = 0,$$

$$p_1 = -0.34790196497952825,\ p_2 = 0.69580392995905650,\ p_3 = 1.0678596267584018.$$

Of course, p_3 can be recovered from the level of energy, which was fixed to

$$h = -1.2929708570.$$

The corresponding period is close to 2π. Of course, by the homogeneity of the potential, any period or any negative value of h are equivalent.

Now everything is prepared to carry out the algorithm described in section 4. The computations are done using multiprecision intervals with 200 bits of mantissa. For ODE integration we used Taylor method of order 50. As a result we obtained very sharp rigorous enclosures for the initial conditions of the Eight

$$\boldsymbol{x} = (1.990983769917805^{3}_{2},\ 0.995491884958902^{7}_{6},\ -0.347901964963102^{20}_{19},\ 0.695803929926204^{40}_{39})$$

Next we computed the Taylor expansion of the Poincaré map at the fixed point $\hat{x} \in \boldsymbol{x}$ and we proved that all eigenvalues of the linear part lie on the unit circle. Their rigorous estimates are:

$$\boldsymbol{\lambda}_1, \boldsymbol{\lambda}_3 = 0.998599982092038^{4}_{3} \mp \mathrm{i}\, 0.052896840792060^{7}_{6}$$

$$\boldsymbol{\lambda}_2, \boldsymbol{\lambda}_4 = -0.297596667518713^{30}_{29} \pm \mathrm{i}\, 0.954691690275848^{5}_{4}$$

The final normal form is

$$\begin{pmatrix} z_1 \\ z_2 \\ z_3 \\ z_4 \end{pmatrix} \mapsto \begin{pmatrix} \lambda_1 z_1 + c_{11} z_1^2 z_3 + c_{12} z_1 z_2 z_4 \\ \lambda_2 z_2 + c_{21} z_1 z_2 z_3 + c_{22} z_2^2 z_4 \\ \lambda_3 z_4 + c_{31} z_1 z_3^2 + c_{32} z_2 z_3 z_4 \\ \lambda_4 z_4 + c_{42} z_1 z_3 z_4 + c_{41} z_2 z_4^2 \end{pmatrix} \tag{7}$$

where

$$\begin{aligned} c_{11} &\in -235.97^{5}_{4} + \mathrm{i}\, 12.^{500}_{499}, & c_{12} &\in 22.02^{4}_{3} - \mathrm{i}\, 1.16^{7}_{6}, \\ c_{21} &\in -6.56^{4}_{3} + \mathrm{i}\, 21.05^{6}_{5}, & c_{21} &\in -0.15^{2}_{1} + \mathrm{i}\, 0.48^{7}_{6}, \\ c_{31} &\in 235.97^{5}_{4} + \mathrm{i}\, 12.^{500}_{499}, & c_{32} &\in -22.02^{4}_{3} - \mathrm{i}\, 1.16^{7}_{6}, \\ c_{42} &\in 6.56^{4}_{3} + \mathrm{i}\, 21.05^{6}_{5}, & c_{41} &\in 0.15^{2}_{1} + \mathrm{i}\, 0.48^{7}_{6}. \end{aligned}$$

Due to the form of the eigenvalues and to the fact that no resonances appear to order 3, except the unavoidable ones, and using the fact that the second and fourth variables are related to the complex conjugates of the first and third ones, we only need to work with the two complex variables z_1, z_2.

At this point the map reads as

$$\begin{pmatrix} z_1 \\ z_2 \end{pmatrix} \mapsto \begin{pmatrix} \lambda_1 z_1 + c_{11} |z_1|^2 z_1 + c_{12} |z_2|^2 z_1 \\ \lambda_2 z_2 + c_{21} |z_1|^2 z_2 + c_{22} |z_2|^2 z_2 \end{pmatrix}. \tag{8}$$

Let us write $\lambda_j = \exp(i 2\pi \alpha_j)$ for $j = 1, 2$. Then the map can be written in the form

$$\begin{pmatrix} z_1 \\ z_2 \end{pmatrix} \mapsto \begin{pmatrix} z_1 \exp(i2\pi(\alpha_1 + d_{11}|z_1|^2 + d_{12}|z_2|^2)) \\ z_2 \exp(i2\pi(\alpha_2 + d_{21}|z_1|^2 + d_{22}|z_2|^2)) \end{pmatrix}, \tag{9}$$

where $d_{jk} = c_{jk}/\lambda_j$ for $j = 1, 2,\ k = 1, 2$. In the above expression we let aside, as in all the computations, terms of order 4 or higher. To obtain (9) we take first $\lambda_1 z_1$ and $\lambda_2 z_2$ as factors in (8) and compute logarithms. Note that the values of the coefficients d_{jk}, $j = 1, 2$, $k = 1, 2$ must be real, although from rigorous computations we get complex intervals around some real point. It should also hold that the matrix formed by the d_{jk} coefficients is symmetric, a fact which is compatible with the results obtained in the computations.

For the figure eight orbit we have

$$\begin{aligned} d_{11} &\in -37.6^{10}_{09} + \mathrm{i}\, {}^{+0.001}_{-0.001}, & d_{12} &\in 3.51^{1}_{0} + \mathrm{i}\, {}^{+0.001}_{-0.001}, \\ d_{21} &\in 3.51^{1}_{0} + \mathrm{i}\, {}^{+0.001}_{-0.001}, & d_{22} &\in 0.08^{2}_{1} + \mathrm{i}\, {}^{+0.001}_{-0.001}. \end{aligned}$$

For the map (9) the non-degeneracy KAM condition is simply that the determinant of the torsion $d = d_{11}d_{22} - d_{12}d_{21}$ must be different from zero. Because for the Eight we have

$$d \in \boldsymbol{d} = -15.37^{3}_{2} + \mathrm{i}\, {}^{+0.001}_{-0.001}$$

this finishes the proof that it is KAM stable on the level of fixed energy and angular momentum $M = 0$.

5.3. **Stability of rotating Eights.** Exactly the same algorithm as for the figure eight orbit can be used for the rotating Eights introduced in section 3.2. The obtained Birkhoff normal form and torsion condition are the same. Therefore, keeping the same notation as in the previous section, we only list in Table 2 the rigorous estimates that verify KAM stability of rotating Eights for the two selected values of angular momentum $M_1 = 0.0048828125$ and $M_2 = 0.1484375$.

M	0.0048828125	0.1484375000
$\boldsymbol{x}$	$\begin{pmatrix} 1.990931659347265^{6}_{5} \\ 1.008912014249292^{1}_{0} \\ -0.3572035647908583^{4}_{3} \\ 0.6959444683858283^{4}_{3} \end{pmatrix}$	$\begin{pmatrix} 1.9515112915449305^{5}_{4} \\ 1.375174867045771^{9}_{8} \\ -0.7065769953712015^{5}_{4} \\ 0.8355362677548005^{5}_{4} \end{pmatrix}$
$\mathrm{diam}(\boldsymbol{x})$	10^{-52}	$2 \cdot 10^{-30}$
$\boldsymbol{\lambda_1}, \boldsymbol{\lambda_3}$ $\boldsymbol{\lambda_2}, \boldsymbol{\lambda_4}$	$0.998512197^{7}_{6} \mp \mathrm{i}\, 0.0545288^{5}_{4}$ $-0.2987453^{2}_{1} \pm \mathrm{i}\, 0.9543328^{2}_{1}$	$0.6540184^{7}_{6} \mp \mathrm{i}\, 0.75647^{600}_{599}$ $-0.6209225^{5}_{4} \pm \mathrm{i}\, 0.7838719^{5}_{4}$
$\boldsymbol{D} = (\boldsymbol{d_{jk}})$	$\begin{pmatrix} -36.39^{5}_{4} + \mathrm{i}^{\,+0.001}_{-0.001} & -3.50^{6}_{5} + \mathrm{i}^{\,+0.001}_{-0.001} \\ -3.50^{6}_{5} + \mathrm{i}^{\,+0.001}_{-0.001} & 0.08^{9}_{8} + \mathrm{i}^{\,+0.001}_{-0.001} \end{pmatrix}$	$\begin{pmatrix} -0.5^{50}_{49} + \mathrm{i}^{\,+0.001}_{-0.001} & 3.28^{1}_{0} + \mathrm{i}^{\,+0.001}_{-0.001} \\ 3.28^{1}_{0} + \mathrm{i}^{\,+0.001}_{-0.001} & 1.55^{8}_{7} + \mathrm{i}^{\,+0.001}_{-0.001} \end{pmatrix}$
$\boldsymbol{d} = det(\boldsymbol{D})$	$-15.49^{7}_{6} + \mathrm{i}^{\,+0.001}_{-0.001}$	$-11.61^{8}_{7} + \mathrm{i}^{\,+0.001}_{-0.001}$

TABLE 2. Rigorous estimates of the initial condition $\boldsymbol{x}$, eigenvalues $\boldsymbol{\lambda_i}$ and torsion $\boldsymbol{d}$ for the proof of KAM stability of rotating Eights with angular momentum $M_1 = 0.0048828125$ and $M_2 = 0.1484375$.

6. Acknowledgements

The research of T.K. was supported in part by Polish Ministry of Science and Higher Education through grant N201 024 31/2163. The work of C.S. was supported by grants MTM2006-05849/Consolider (Spain) and 2009 SGR 67 (Catalonia).

References

[1] G. Alefeld. Inclusion methods for systems of nonlinear equations–the interval Newton method and modifications. *Topics in Validated Computations*, pages 7–26, 1994.
[2] V. I. Arnold. Proof of A. N. Kolmogorov's theorem on the preservation of quasi-periodic motions under small perturbations of the Hamiltonian. *Usp. Mat. Nauk SSSR*, 18:13–40, 1963.
[3] V. I. Arnold and A. Avez. *Problèmes ergodiques de la mécanique classique*. Gauthier-Villars, Paris, 1967.
[4] O. Bohigas, S. Tomsovic, and D. Ullmo. Manifestations of classical phase space structures in quantum mechanics. *Physics Reports*, 223:43–133, 1993.
[5] CAPD. CAPD - Computer Assisted Proofs in Dynamics, a package for rigorous numerics.
[6] A. Chenciner, J. Gerver, R. Montgomery, and C. Simó. Simple Choreographic Motions of N Bodies: A Preliminary Study. *Geometry, Mechanics and Dynamics, Springer-Verlag*, pages 287–308, 2002.
[7] A. Chenciner and R. Montgomery. A remarkable periodic solution of the three body problem in the case of equal masses. *Annals of Mathematics*, 152:881–901, 2000.
[8] G. G. de Polavieja, F. Borondo, and R. M. Benito. Scars in Groups of Eigenstates in a Classically Chaotic Sistem. *Physical Review Letters*, 73:1613–1616, 1994.
[9] M. Hénon. Private communication. 2000.
[10] T. Kapela and C. Simó. Computer assisted proofs for nonsymmetric planar choreographies and for stability of the Eight. *Nonlinearity*, 20(5):1241–1255, 2007.
[11] T. Kapela, C. Simó, and P. Zgliczyński. Some properties of the Hénon map in the 3:1 resonance. *In preparation*, 2011.
[12] T. Kapela and P. Zgliczyński. The existence of simple choreographies for the N-body problem—a computer-assisted proof. *Nonlinearity*, 16(6):1899–1918, 2003.
[13] R.B. Kearfott, M.T. Nakao, A. Neumaier, S.P. Shary, and P. van Hentenryck. Standardized notation in interval analysis. *Proc. XIII Baikal International School-seminar "Optimization methods and their applications", Irkutsk, Baikal, July 2-8, 2005*, 4, 2005.

[14] A. N. Kolmogorov. On the conservation of conditionally periodic motions under small perturbations of the Hamiltonian. *Dokl. Akad. Nauk SSSR*, 98:527–530, 1954.
[15] R. Krawczyk. Newton-Algorithmen zur Bestimmung von Nullstellen mit Fehlerschranken. *Computing (Arch. Elektron. Rechnen)*, 4:187–201, 1969.
[16] R. J. Lohner. Einschliessung der lsung gewonhnlicher anfangs- and randwertaufgaben und anwendungen. *Universitt Karlruhe (TH) these*, 1988.
[17] R. Martínez and A. Samà. On the centre manifold of collinear points in the planar three-body problem. *Celestial Mechanics & Dynamical Astronomy*, 85:311–340, 2003.
[18] C. Moore. Braids in Classical Gravity. *Physical Review Letters*, 70:3675–3679, 1993.
[19] R. E. Moore. *Interval analysis*. Prentice-Hall Inc., Englewood Cliffs, N.J., 1966.
[20] J.J. Morales and J.P. Ramis. A note on the non-integrability of some Hamiltonian systems with a homogeneous potential. *Methods and Applications of Analysis*, 8:113–120, 2001.
[21] J. K. Moser. On invariant curves of area-preserving mappings of an annulus. *Nachr. Akad. Wiss. Göttingen, math.-phys. Kl.*, 11a:1–20, 1962.
[22] A. Neumaier. *Interval methods for systems of equations*. Cambridge Univ. Press, 1990.
[23] J. Puig and C. Simó. Resonance tongues in the Quasi-Periodic Hill-Schrödinger Equation with three frequencies. *Regular and Chaotic Dynamics*, 16:62–79, 2011.
[24] C. Simó. Dynamical properties of the figure eight solution of the three-body problem. *Contemporary Mathematics AMS*, 292:209–228, 2000.
[25] C. Simó. New families of Solutions in N–Body Problems. *Proc. 3rd ECM, 2000, Progress in Mathematics series, Birkäuser*, 210:101–115, 2001.
[26] C. Simó and A. Vieiro. Resonant zones, inner and outer splittings in generic and low order resonances of Area Preserving Maps. *Nonlinearity*, 22:1191–1245, 2009.
[27] E. T. Whittaker. *A treatise on the Analytical Dynamics of Particles and Rigid Bodies*. Cambridge Univ. Press, 1970, fourth edition, reprinted.
[28] D. Wilczak and P. Zgliczyński. C^r-Lohner algorithm. *Schedae Informaticae*, 20:9–46, 2011.
[29] P. Zgliczynski. C^1-Lohner algorithm. *Foundations of Computational Mathematics*, 2:429–465, 2008.

Tomasz Kapela, Jagiellonian University, Institute of Computer Science, Nawojki 11, 30-072 Kraków, Poland, Uppsala University, Department of Mathematics, Box 480, 75106 Uppsala, Sweden
E-mail address: kapela@ii.uj.edu.pl

Carles Simó, Dept. de Matemàtica Aplicada i Anàlisi, Univ. de Barcelona, Gran Via 585, 08007 Barcelona, Spain
E-mail address: carles@maia.ub.es